ACS Energy LETTERS

http://pubs.acs.org/journal/aelccp

LETTER

Nonintuitive Role of Solid Electrolyte Porosity on Failure

Lin Lin, Abhinand Ayyaswamy, Yanjie Zheng, Austin Fan, Bairav S. Vishnugopi, Partha P. Mukherjee, and Kelsey B. Hatzell*

Cite This: *ACS Energy Lett.* 2024, 9, 2387−2393

Read Online

ACCESS | Metrics & More | Article Recommendations | Supporting Information

ABSTRACT: **Solid electrolyte failure can occur through a range of different mechanisms. Electrochemical delamination at electrode and electrolyte interfaces is a prominent failure mechanism during high capacity and low N/P operating conditions, and filament formation is prevalent during a high rate and long cycle-life deposition. Interface coherency and the solid electrolyte microstructure both impact the ultimate degradation mode. The solid electrolyte microstructure, described in part by the density, periodicity, and interconnected arrangement of pores, plays a role in failure. Herein, we combine modeling, synchrotron imaging, and electrochemical experiments to systematically understand how densification and processing of solid electrolytes influence filament formation. The work reveals that the density of pores is not correlated with failure. Instead, the periodicity, size, and arrangement of pores is a driver for failure in amorphous solid electrolytes absent of grain boundaries.**

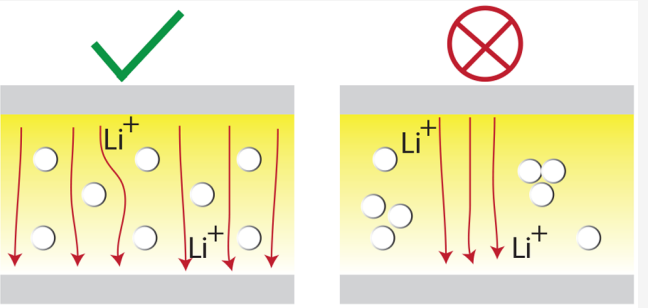

Solid state batteries, which incorporate alkali metal anodes, represents a promising route toward energy dense batteries for electric vehicle applications.[1,2] Significant innovation and discovery in new families of solid electrolytes have yielded new materials with exceptional transport properties that rival or exceed the performance of conventional liquid electrolytes. Nevertheless, there are still considerable challenges associated with processing and manufacturing solid state batteries that can operate at high rates and long cycle lifetimes.[3,4] Manufacturing solid state components for controlled extrinsic interfaces (cathodelsolid electrolyte) and with a controlled microstructure remains a significant challenge.

Solid electrolytes are usually processed using high temperature solid state sintering approaches or cold pressing to achieve dense structures.[5−8] High-temperature sintering approaches are mainly employed in the fabrication of oxide solid electrolytes such as garnets, NASICON, perovskite, etc., in which cases high temperature exposure is a necessity to enable mass diffusion driven densification. On the other hand, cold pressing to achieve high densification of pellets, widely studied in the pharmaceutical industry in the development of tablets,[9] has been widely utilized in the densification process of softer solid electrolytes, including sulfides, argyrodites, halides, etc. Pressure, temperature, particle size, and particle size distribution can all affect the compactability of a powder into a component or part.[10] The residual porosity and pore size distribution (e.g., microstructure) can play a large role on a component's effective mechanical properties, performance, and degradation mechanisms. High density (low porosity) solid electrolytes can result in higher ionic conductivity, while low density (high porosity) often results in lower ionic conductivity.[10−12] While there is a clear relationship between porosity and solid electrolyte ionic conductivity, the role that microstructure plays on degradation is less understood. Recently, filament formation and growth in solid electrolytes has been described by a range of solid electrolyte properties including the solid electrolyte electronic conductivity,[13] solid electrolyte pore connectivity,[14−18] and interface discontinuities and defects.[19] In reality, there is likely an ensemble of electro−chemo−mechanical phenomenon, driven by external operating conditions and microstructure, which contribute to solid electrolyte failure. Stress at interfaces and within the bulk can result in "hot spots" for ion transport and high local current densities, which can further drive stress gradients across a solid

Received: March 14, 2024
Revised: April 13, 2024
Accepted: April 18, 2024
Published: April 24, 2024

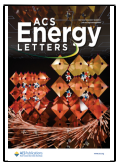

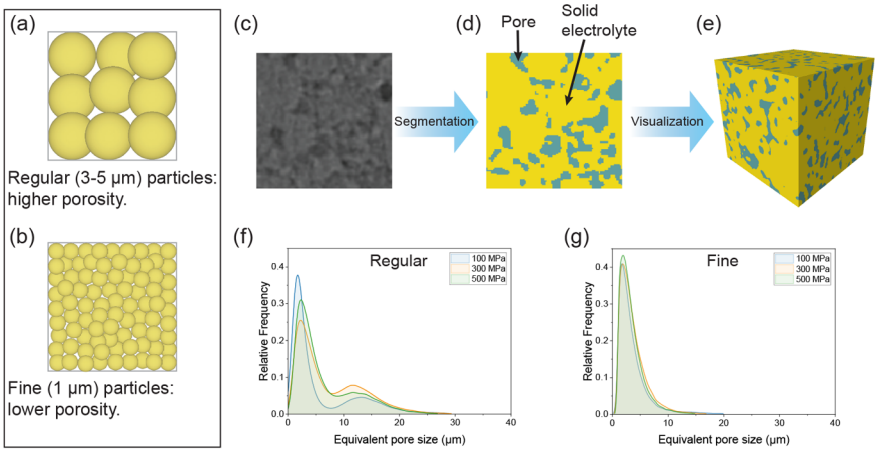

Figure 1. Schematic illustration of particle size effect on densification. Large particles induce higher porosity (a), whereas smaller particles yield lower porosity (b). Binarized 2D images (c) can be segmented (d) and reconstructed into a 3D visualization of solid electrolyte structure (e). Subvolumes are used to capture pore size distribution for powders with regular particles (f) and fine particles (g) at 100, 300, and 500 MPa.

electrolyte. Furthermore, lithium metal deposition and growth within a solid electrolyte will progress along directions of least resistance which may be grain boundaries[20,21] or pores.[17,22] The size, distribution, and arrangement of pores and grain boundaries all contribute to the magnitude of stress generated and ultimate failure mode (fracture or shorting). Recently, Diallo et al. revealed a nonmonotonic relationship between the time for a solid electrolyte shorted and the solid electrolyte density. Shorting was ascribed to percolation networks of pores. However, above a certain density threshold (>95%) pores played little role on failure.

To systematically study the role of microstructure on degradation mechanisms, we processed argyrodite solid electrolytes Li_6PS_5Cl (LPSCl) from powders with varying sizes (1−5 μm) and varying pressures ranging from 100 to 500 MPa via cold uniaxial pressing. Synchrotron X-ray tomography was implemented with 3-D volumetric quantification approaches to evaluate structural and transport heterogenity. Electrochemical experiments reveal porosity independent critical current densities. The microstructure and degree of heterogeneity influences ion-transport pathways and the subsequent nonuniformity in current distribution at the electrode-solid electrolyte interfaces. The work reveals that ultimately the organization and periodicity of pores is more impactful on failure rather than the absolute density of pores. Although this work primarily focuses on argyrodite LPSCl, we believe the interpretation of ionic transportation affected by pore distribution is universally applicable to other solid electrolyte systems fabricated via different processing routes.

The particle size and distribution can impact how the material densifies under an applied load. Typically, materials with a bimodal distribution of particle size experience a greater level of compaction or packing density. The presence of two different sizes can enable a greater propensity for particle rearrangement and deformation leading to a denser component.[23] To systematically examine how compaction and microstructure influence degradation mechanisms, we examined a series of LPSCl solid electrolytes processed with powders with varying particles (1 to 5 μm) and varying pressures (100, 300, and 500 MPa). In this study we refer to regular powders as powder with particle sizes from 3 to 5 μm and fine powders as powders with particles sizes around 1 μm (Figure 1(a) and (b)). Scanning electron microscopy images of the two types of powders (Figure S1) confirm such particle size distribution.

Using synchrotron-based attenuation contrast tomography, it is possible to resolve the porous region of the solid electrolyte from the solid electrolyte within the resolution limit of the technique (~1 μm). Lighter regions have a higher attenuation and are the solid region (e.g., LPSCl) and darker regions have a lower attenuation and are the porous region. Two-dimensional radiographs can be segmented and reconstructed into a three-dimensional image for quantitative volumetric analysis (Figure 1(c)−(e)). Compared to other imaging techniques such as focused ion beam scanning electron microscopy, X-ray tomography provides nondestructive characterizations over a larger range of sample which yields better statistics. However, the spatial resolution (0.92 μm in our case) possibly limits the detection and quantification of very small pores, and segmentation based on grayscale attenuation contrast may post ambiguity at some "gray" voxels. The volumetric analysis suggests that regular powders with particle sizes between 3 and 5 μm exhibit a bimodal distribution with a high density of pores between 1 and 2 μm and a high density of pores between 10 and 12 μm. It should be noted that the resolution of the imaging is 0.92 μm, so it is impossible to resolve pores that fall below that spatial resolution. The absolute magnitude of size of the pores is similar in all the solid electrolyte. However, it should be noted that the frequency is normalized to the total number of pores identified. Thus, it was observed that the density of small pores increases with applied pressure for both solid electrolytes. The solid electrolyte composed of fine particles demonstrates a uniform pore size distribution, which is indicative of a denser solid electrolyte.

The overall porosities of different samples are also readily obtained from the 3D-volume segmentation results (Table S1). Generally, the solid electrolyte samples pressed from regular particles show porosities from 13.9 to 17.9%, while porosities from fine particles are from 6.1 to 9.5%. These values agree with the relative density values reported in previous literature,[24] as well as direct relative porosity measurements based on geometric dimensions and masses of pellets (also included in Table S1). Statistical analysis accross a range of

https://doi.org/10.1021/acsenergylett.4c00744
ACS Energy Lett. 2024, 9, 2387−2393

different subvolume sizes (Figure S3) suggest that small subvolume sizes (e.g., 92 μm) yields high standard deviations of porosity values. On the other hand, as the subvolume increases, the standard deviation significantly decreases to ~0.5% for the large 460 μm × 460 μm × 460 μm volumes of interest, which are likely sufficient to represent the total porosities in solid electrolytes.[15] It has therefore been indicated that denser LPSCl solid electrolyte pellets can be achieved by the utilization of smaller particles and pressing at higher pressure values, agreeing with the powder compaction theory (Figure 1a).

The solid electrolyte microstructure is critical for ionic conductivity, but it also plays a significant role in the distribution of stress at extrinsic interfaces that form between an electrode and the solid electrolyte.[25] Discontinuities at the electrode and the solid electrolyte can lead to current focusing and increase in constriction resistances.[26−29] High local ionic flux toward an interface can lead to the formation of dendrites or filaments and high local ionic flux away from an electrode can result in voiding and a decrease in contact surface area.[29−33] Both of these mechanisms can contribute to electrical shorting due to filament growth and fracture.

Prior work by Diallo et al. revealed that filament formation was related to pore connectivity and solid electrolyte density.[16] Solid electrolytes with densities beyond 95% demonstrate a greater critical current density, and solid electrolytes with densities less than 95% demonstrate a critical current density highly dependent on the pore connectivity. Critical current density tests are often used to explore the power performance of the cell but can be highly misleading when used exclusively to understand the power performance and attainable currents. Herein, we use a conventional critical current density test where we cycle Li|LPSCl|Li symmetric cells at different current densities as a simple control experiment to understand how solid electrolyte microstructure evolves as the current density is increased (Figure 2). To get reliable critical current density

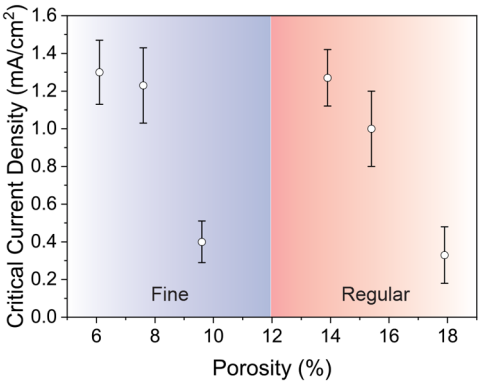

Figure 2. Critical current density trend as a function of porosity, in both regular and fine solid electrolyte cases. The CCD does not increase monotonically with decreasing porosity.

statistics, for each particle size and pressure combination, we have assembled three cells and run the exact same testing. Both the fine particles and regular particles show an increase in critical current density (or current density observed at failure onset) with an increase in processing pressure (decreasing porosity). Low critical current densities around 0.3 to 0.4 mA/cm^2 for regular and fine particles densified at 100 MPa are observed. When the pressure increases to 300 and 500 MPa, the critical current density exceeds 1 mA/cm^2 for both the solid electrolytes processed from fine and regular powders. The highly dense solid electrolyte processed from fine particles has a slightly greater critical current density when compared to the less dense solid electrolyte composed of regular solid electrolyte particles densified at the same pressure. Both particles (fine and regular) exhibit an increase in critical current density with densitification pressure, yet the trend does not correlate with absolute solid electrolyte porosity. Similar critical current densities are observed for solid electrolytes with vastly different densities. This discrepancies suggests that the underlying microstructure is tied to filament growth in these solid electrolytes.

Volumetric quantification of each solid electrolyte subvolume reveals local structural heterogeneity across the thickness of the solid electrolyte. The z-direction of the solid electrolyte represents the driving force direction of densification (e.g., compression). Porosity variation as a function of z-axis position reveals a nonuniform distribution of pores (Figure 3a) that is reflected by the standard deviations of porosity (Table S1). The porosity through the thickness of the solid electrolytes processed with fine particles is fairly uniform. Large deviations observed at the interface for the fine powders (e.g., 400 μm) are likely an artifact of a tilted sample in the X-ray beam (Figure 3(a)). The porosity through the thickness of the solid electrolyte processed with regular particles is highly heterogeneous and is in agreement with prior observations that the pore size distribution is bimodal in nature.

To further understand the structural heterogeneities in the xy-directions (i.e., compression direction), we calculated the structure factor for each solid electrolyte (Figure 3(b)−(g)). The structure factor evaluates the difference of the local porosity at a specific (x,y) position along the whole z-axis compared to the overall porosity throughout the sample, and a number closer to zero corresponds to a more uniform solid electrolyte in the (x,y) plane. The solid electrolytes fabricated from fine particles at all pressures yield smaller structure factors than the solid electrolytes fabricated from regular particles. suggesting more homogeneous pore distributions. The increasing fabrication pressure also assists in reaching a more homogeneous solid electrolyte in terms of xy plane porosity distribution. For both the solid electrolyte pressed from regular particles (Figure 3(b)−(d))and fine particles (Figure 3(e)−(g), an overall lower structure factor value is associated with the increasing pressure from 100 to 500 MPa, indicating the decrease of porosity variation at different (x,y) locations.

The lithium ion transport pathways in the solid electrolyte systems with the heterogeneities discussed above are further evaluated by tortuosity measurements. In solid electrolyte systems, the tortuosity factor is correlated to degradation mechanism; its heterogeneity correlates to the Li plating/stripping "hot spots" on the interface, which directly affects the filament formation and growth behavior.[14] The results are summarized in Figure 4. It can be observed that the tortuosity values for solid electrolytes pressed with regular particles (1.17 to 1.30) are generally higher than those pressed with fine particles (1.05 to 1.13), and a general decreasing trend in tortuosity factors can be observed with increasing fabrication pressure. Moreover, to study the spatial heterogeneities of tortuosity factors, the 460 × 460 × 460 μm^3 volume of interest in each solid electrolyte was further divided into 64 (4 × 4 × 4) subvolumes, and the tortuosity factor for each subvolume was calculated, generating the standard deviation of tortuosity

https://doi.org/10.1021/acsenergylett.4c00744
ACS Energy Lett. 2024, 9, 2387−2393

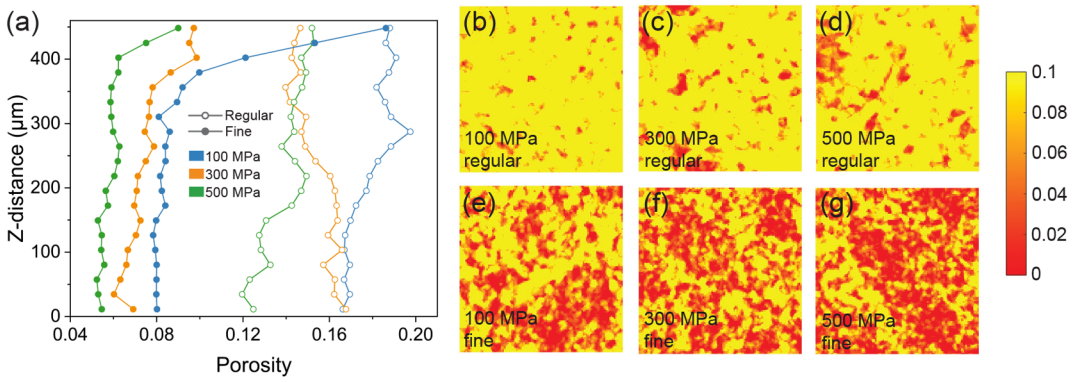

Figure 3. Structural analysis of solid electrolyte. (a) The overall porosity along *z*-direction. (b)−(g) Structure factors of LPSCl solid electrolytes pressed from different sized particles at different pressures: (b) regular particles, 100 MPa, (c) regular particles, 300 MPa, (d) regular particles, 500 MPa, (e) fine particles, 100 MPa, (f) fine particles, 300 MPa, (g) fine particles, 500 MPa. The field-of-view analyzed is 100 μm × 100 μm for each case.

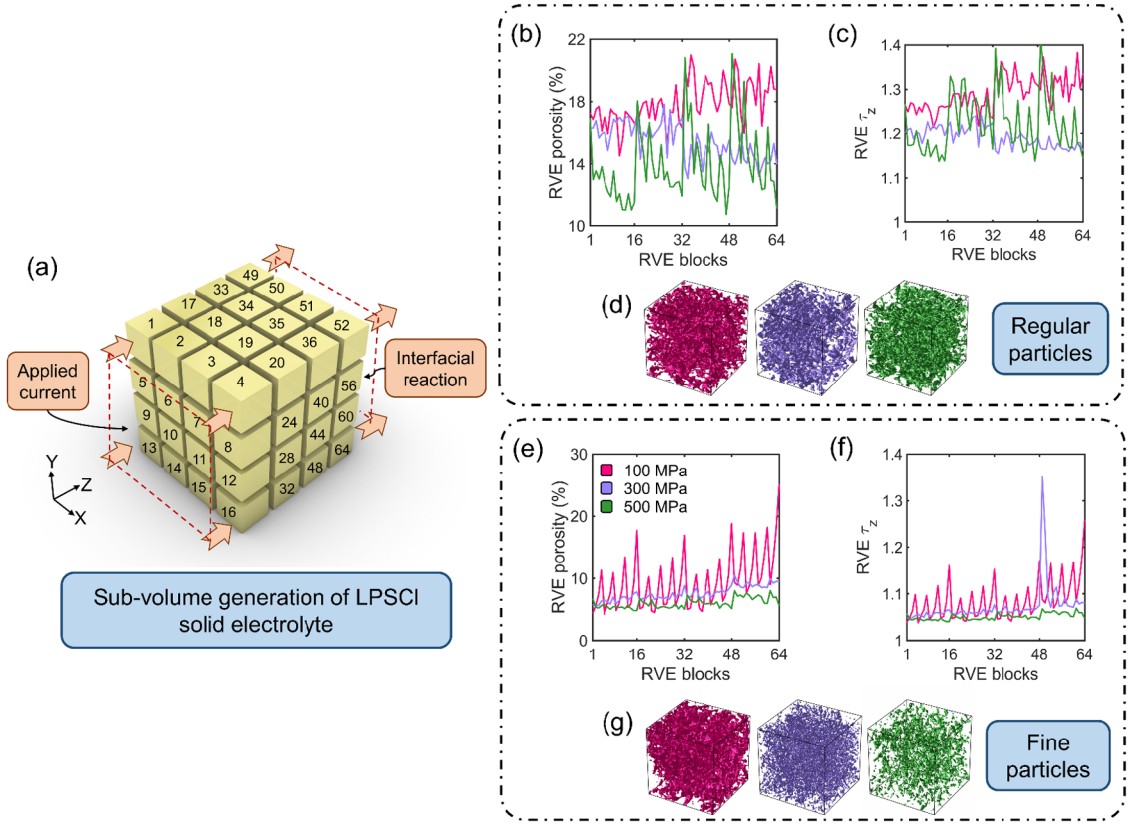

Figure 4. Assessment of ionic transport in a heterogeneous distribution of LPSCl solid electrolyte (SE) particles obtained from X-ray tomograms. (a) Schematic of 64 generated representative volumetric element (RVE) treated as subvolumes of SE. The X-ray tomograms of the SE have a resolution of 500 × 500 × 500 points with a voxel size of 0.92 μm. The *z*-axis points to the direction of ionic flux in the SE. Variation in (b),(e) RVE porosity and (c),(f) RVE tortuosity in the *z*-direction with associated RVE blocks of regular and fine particles for three manufacturing pressures of 100, 300, and 500 MPa. 3D visualization of the pore network in LPSCl for (d) regular and (g) fine particles at 100, 300, and 500 MPa, respectively. The subvolume size shown is of dimensions 115 × 115 × 115 μm^3.

for each solid electrolyte. An interesting finding is that the standard deviations of tortuosity factors in solid electrolytes pressed at 100 MPa are significantly higher than those pressed at higher pressures, and the fine powder-100 MPa fabricated sample yields very high tortuosity standard deviations (4% to 8%) despite the relatively low overall porosity (9.5%). This is possibly connected to its anomalous electrochemical behavior, which will be further discussed in the following section.

The stochastic distribution of particle and pore network in the SE for various manufacturing pressures (100, 300, and 500 MPa) and particle sizes (regular, fine) facilitates drastic variations in the ionic transport through its relative transport properties. To evaluate the microstructure-induced transport variations, we performed a finite volume 3D direct numerical simulation on 64 subvolumes of size 115μm × 115μm × 115 μm (Figure 4a). These subvolumes are treated as representa-

https://doi.org/10.1021/acsenergylett.4c00744
ACS Energy Lett. 2024, 9, 2387−2393

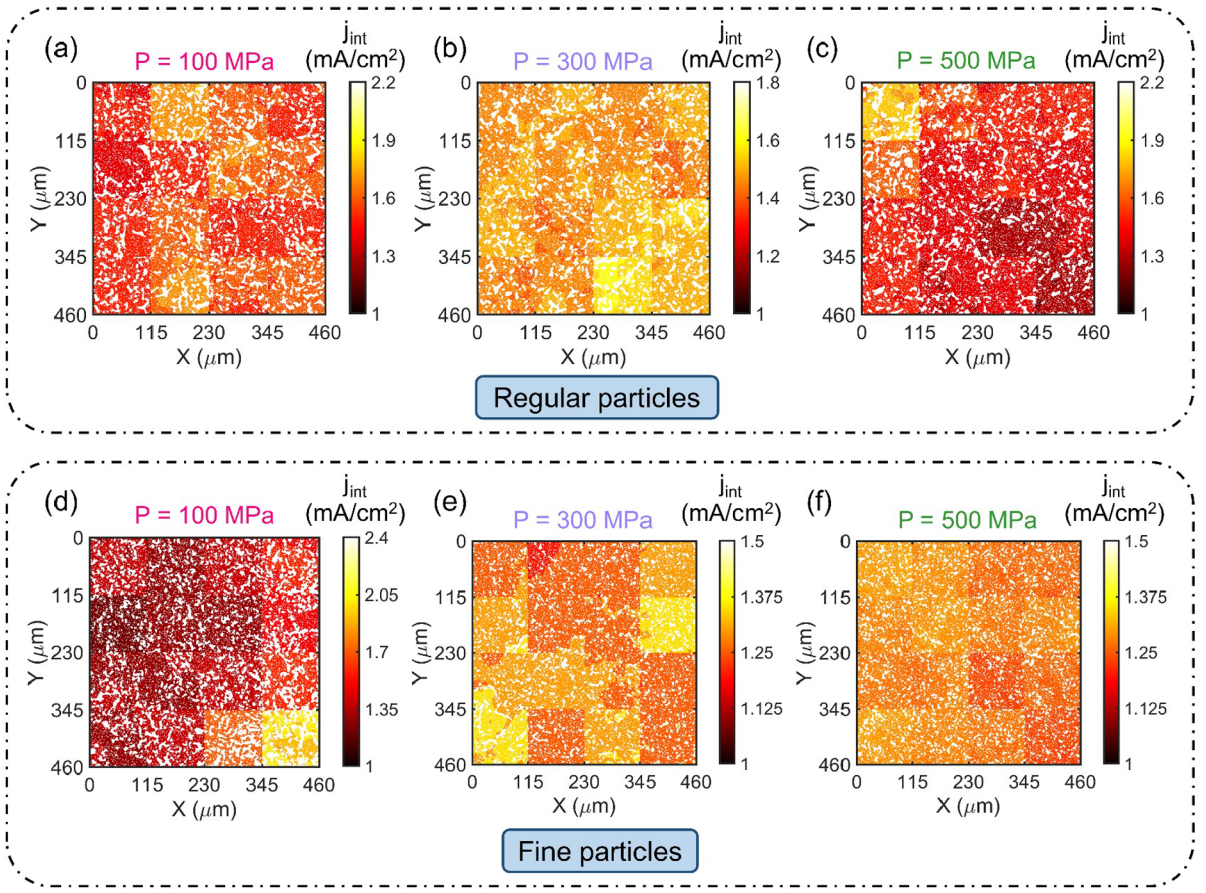

Figure 5. Quantification of interfacial current densities and the associated reaction heterogeneities at the anode−SE interface for (a) regular particles, 100 MPa, (b) regular particles, 300 MPa, (c) regular particles, 500 MPa, (d) fine particles, 100 MPa, (e) fine particles, 300 MPa, and (f) fine particles, 500 MPa.

tive volumetric element blocks where the transport properties are evaluated by solving the Laplace equation based on the pore-particle arrangement in these RVEs. A detailed description of the governing equations and methodology is described in Section S1 of the Supporting Information. Figure 4(b),(c) indicates the variation of RVE porosity and tortuosity in the z-direction for regular particles at various pressures. We observe that SE manufactured under high pressures have a denser particle arrangement, resulting in overall lower porosity across all the RVE blocks. Proportionately, the regular particles at 100 MPa have the highest mean tortuosity since the ion percolating network is purely a function of the SE particle network. Although the overall trend of higher tortuosity with lower pressure exists even with fine particles, Figure 4(e),(f) shows a stark contrast in the block-to-block variation of porosity and tortuosity in fine particles at 100 MPa. We identify that the in-plane and through-plane tortuosity of fine particles at 100 MPa exceed those of regular particles at all pressures stemming from significant variation in RVE porosity throughout the SE (see Figure S7). This distinction in the pore percolation network across various pressures (Figure 4(d),(g)) manifests as greater heterogeneity in ionic transport throughout the SE that could potentially dictate its critical current density.

We further validated our hypothesis by analyzing the distribution of interfacial reaction kinetics at the anode−SE interface. To this end, we modeled the electric potential distribution in the SE by applying a constant current (J_{app} = 1 mA/cm^2) to 16 subvolumes (RVE 1−16), with an initial 93.06% contact with the anode (RVE 49−64) as shown in Figure 4(a). More details on the governing equations and methodology are described in the Experimental and Computational Method section in the Supporting Information. Hypothetically, a 100% dense SE with a smooth surface would result in a mean reaction current of 1.07 mA/cm^2 at the anode−SE interface proportional to its initial interfacial contact. However, the presence of pores and the relative distribution of SE particles affects the electric potential distribution, thus increasing the magnitude of current at the anode−SE interface. Figure 5(a)−(c) shows the relative magnitude and heterogeneity in current density at the interface (at Z = 460 μm) for regular particles. We observe that higher pressures result in a denser SE network with a homogeneous current distribution at the interface. This effect is more pronounced in fine particles (Figure 5(e),(f), where higher pressures result in homogenization of reaction currents with lower magnitudes in comparison with regular particles. However, under low pressures, microstructures have a denser pore network impeding overall ionic transport resulting in large potential gradients and high currents. We critically examine the impact of higher block-to-block variance in the porosity and tortuosity of fine particles at 100 MPa in Figure 5(e). This manifests as very high reaction currents (J_{int} = 2.4 mA/cm^2) in certain regions of the SE, thus exhibiting maximum

https://doi.org/10.1021/acsenergylett.4c00744
ACS Energy Lett. 2024, 9, 2387−2393

heterogeneity among all the examined cases (see Figure S8). The presence of high reaction currents and heterogeneity implies uneven loss of interfacial contact during stripping and subsequent plating, resulting in unexpected drop of critical current densities. The overall microstructure of SE governed by the particle size and its manufacturing pressure dictates the local porosity and tortuosity. Hence, the local variation and distribution of ion-transport networks stemming from its structural properties govern the overall electrochemical performance of SE and cannot be understood solely from its global porosity.

Herein, we systematically investigate how solid electrolyte processing influences failure mechanisms by using argyrodite LPSCl as a model system. Our work reveals that solid electrolyte failure via filament propagation is not tied uniquely to the absolute density of pores in a solid electrolyte. Instead, the failure mode is tied to the periodicity of the pores in a solid electrolyte. Prior work has shown how lithium filaments tend to grow through connected pores or grain boundaries. In amorphous or glass type solid electrolytes, the arrangement of pores is often challenging to control with conventional cold pressing experiments. Synchrotron X-ray tomography reveals how pore size, pore size distribution, and directional tortuosity are all influenced by the densification pressure and powder size. Ultimately, the microstructure and degree of heterogeneity influences current nonuniformity at anode interfaces and is the primary driver for degradation.

■ ASSOCIATED CONTENT

Supporting Information

The Supporting Information is available free of charge at https://pubs.acs.org/doi/10.1021/acsenergylett.4c00744.

Experimental procedures, details on modeling, and additional analysis (PDF)

■ AUTHOR INFORMATION

Corresponding Author

Kelsey B. Hatzell − *Andlinger Center for Energy and the Environment, Princeton University, Princeton, New Jersey 08540, United States; Department of Mechanical and Aerospace Engineering, Princeton University, Princeton, New Jersey 08540, United States;* orcid.org/0000-0002-5222-7288; Email: kelsey.hatzell@princeton.edu

Authors

Lin Lin − *Andlinger Center for Energy and the Environment, Princeton University, Princeton, New Jersey 08540, United States;* orcid.org/0000-0003-0352-0389

Abhinand Ayyaswamy − *Department of Mechanical Engineering, Purdue University, West Lafayette, Indiana 47907, United States;* orcid.org/0009-0007-3952-6287

Yanjie Zheng − *Department of Mechanical and Aerospace Engineering, Princeton University, Princeton, New Jersey 08540, United States*

Austin Fan − *Department of Chemical and Biological Engineering, Princeton University, Princeton, New Jersey 08540, United States*

Bairav S. Vishnugopi − *Department of Mechanical Engineering, Purdue University, West Lafayette, Indiana 47907, United States*

Partha P. Mukherjee − *Department of Mechanical Engineering, Purdue University, West Lafayette, Indiana 47907, United States*

Complete contact information is available at: https://pubs.acs.org/10.1021/acsenergylett.4c00744

Notes

The authors declare no competing financial interest.

■ ACKNOWLEDGMENTS

This work was funded by the DOE Basic Energy Science Energy Frontier Research Center (MUSIC) under DE-SC0023438. This research used resources of the Advanced Photon Source, a U.S. Department of Energy (DOE) Office of Science user facility operated for the DOE Office of Science by Argonne National Laboratory. The authors acknowledge the use of the Imaging and Analysis Center (IAC) operated by the Princeton Materials Institute at Princeton University, which is supported in part by the Princeton Center for Complex Materials (PCCM), a National Science Foundation (NSF) Materials Research Science and Engineering Center (MRSEC; DMR-2011750).

■ REFERENCES

(1) Janek, J.; Zeier, W. G. Challenges in speeding up solid-state battery development. *Nature Energy* **2023**, *8*, 230−240.

(2) Hatzell, K. B.; Chen, X. C.; Cobb, C. L.; Dasgupta, N. P.; Dixit, M. B.; Marbella, L. E.; McDowell, M. T.; Mukherjee, P. P.; Verma, A.; Viswanathan, V.; et al. Challenges in lithium metal anodes for solid-state batteries. *ACS Energy Letters* **2020**, *5*, 922−934.

(3) Wang, M. J.; Carmona, E.; Gupta, A.; Albertus, P.; Sakamoto, J. Enabling "lithium-free" manufacturing of pure lithium metal solid-state batteries through in situ plating. *Nat. Commun.* **2020**, *11*, 5201.

(4) Wang, M. J.; Kazyak, E.; Dasgupta, N. P.; Sakamoto, J. Transitioning solid-state batteries from lab to market: Linking electro-chemo-mechanics with practical considerations. *Joule* **2021**, *5*, 1371−1390.

(5) Zaman, W.; Hatzell, K. B. Processing and manufacturing of next generation lithium-based all solid-state batteries. *Curr. Opin. Solid State Mater. Sci.* **2022**, *26*, No. 101003.

(6) Hatzell, K. B.; Zheng, Y. Prospects on large-scale manufacturing of solid state batteries. *MRS Energy & Sustainability* **2021**, *8*, 33−39.

(7) Balaish, M.; Gonzalez-Rosillo, J. C.; Kim, K. J.; Zhu, Y.; Hood, Z. D.; Rupp, J. L. Processing thin but robust electrolytes for solid-state batteries. *Nature Energy* **2021**, *6*, 227−239.

(8) Schnell, J.; Tietz, F.; Singer, C.; Hofer, A.; Billot, N.; Reinhart, G. Prospects of production technologies and manufacturing costs of oxide-based all-solid-state lithium batteries. *Energy Environ. Sci.* **2019**, *12*, 1818−1833.

(9) Zavaliangos, A.; Galen, S.; Cunningham, J.; Winstead, D. Temperature evolution during compaction of pharmaceutical powders. *Journal of pharmaceutical sciences* **2008**, *97*, 3291−3304.

(10) Garner, S.; Strong, J.; Zavaliangos, A. Study of the die compaction of powders to high relative densities using the discrete element method. *Powder technology* **2018**, *330*, 357−370.

(11) Kodama, M.; Ohashi, A.; Hirai, S. In situ X-ray computational tomography measurement of single particle behavior of sulfide solid electrolyte under high-pressure compression. *Journal of Power Sources Advances* **2020**, *4*, No. 100019.

(12) Garcia-Mendez, R.; Mizuno, F.; Zhang, R.; Arthur, T. S.; Sakamoto, J. Effect of processing conditions of 75Li2S-25P2S5 solid electrolyte on its DC electrochemical behavior. *Electrochim. Acta* **2017**, *237*, 144−151.

(13) Han, F.; Westover, A. S.; Yue, J.; Fan, X.; Wang, F.; Chi, M.; Leonard, D. N.; Dudney, N. J.; Wang, H.; Wang, C. High electronic

conductivity as the origin of lithium dendrite formation within solid electrolytes. *Nature Energy* **2019**, *4*, 187−196.
(14) Dixit, M.; Regala, M.; Shen, F.; Xiao, X.; Hatzell, K. Tortuosity Effects in Garnet-Type Li 7 La 3 Zr 2 O 12 Solid Electrolytes. *ACS Appl. Mater. Interfaces* **2019**, *11*, 2022−2030.
(15) Shen, F.; Dixit, M. B.; Xiao, X.; Hatzell, K. B. Effect of pore connectivity on Li dendrite propagation within LLZO electrolytes observed with synchrotron X-ray tomography. *ACS Energy Letters* **2018**, *3*, 1056−1061.
(16) Diallo, M. S.; Shi, T.; Zhang, Y.; Peng, X.; Shozib, I.; Wang, Y.; Miara, L. J.; Scott, M. C.; Tu, Q. H.; Ceder, G. Effect of solid-electrolyte pellet density on failure of solid-state batteries. *Nat. Commun.* **2024**, *15*, 858.
(17) Ning, Z.; Li, G.; Melvin, D. L.; Chen, Y.; Bu, J.; Spencer-Jolly, D.; Liu, J.; Hu, B.; Gao, X.; Perera, J.; et al. Dendrite initiation and propagation in lithium metal solid-state batteries. *Nature* **2023**, *618*, 287−293.
(18) Perrenot, P.; Fauchier-Magnan, A.; Mirolo, M.; Lecarme, L.; Jouneau, P.-H.; Boulineau, A.; Bayle-Guillemaud, P.; Villevieille, C. Room-Temperature Sintering of Amorphous Thiophosphate Solid Electrolyte (Li3PS4): Coupling Morphological Evolution to Electrochemical Properties. *Adv. Funct. Mater.* **2024**, *34*, No. 2310739.
(19) McConohy, G.; Xu, X.; Cui, T.; Barks, E.; Wang, S.; Kaeli, E.; Melamed, C.; Gu, X. W.; Chueh, W. C. Mechanical regulation of lithium intrusion probability in garnet solid electrolytes. *Nature energy* **2023**, *8*, 241−250.
(20) Cheng, E. J.; Sharafi, A.; Sakamoto, J. Intergranular Li metal propagation through polycrystalline Li6. 25Al0. 25La3Zr2O12 ceramic electrolyte. *Electrochim. Acta* **2017**, *223*, 85−91.
(21) Vishnugopi, B. S.; Dixit, M. B.; Hao, F.; Shyam, B.; Cook, J. B.; Hatzell, K. B.; Mukherjee, P. P. Mesoscale interrogation reveals mechanistic origins of lithium filaments along grain boundaries in inorganic solid electrolytes. *Advanced Energy Materials* **2022**, *12*, 2102825.
(22) Porz, L.; Swamy, T.; Sheldon, B. W.; Rettenwander, D.; Frömling, T.; Thaman, H. L.; Berendts, S.; Uecker, R.; Carter, W. C.; Chiang, Y.-M. Mechanism of lithium metal penetration through inorganic solid electrolytes. *Adv. Energy Mater.* **2017**, *7*, No. 1701003.
(23) Skrinjar, O.; Larsson, P.-L. Cold compaction of composite powders with size ratio. *Acta Mater.* **2004**, *52*, 1871−1884.
(24) Singh, D. K.; Henss, A.; Mogwitz, B.; Gautam, A.; Horn, J.; Krauskopf, T.; Burkhardt, S.; Sann, J.; Richter, F. H.; Janek, J. Li6PS5Cl microstructure and influence on dendrite growth in solid-state batteries with lithium metal anode. *Cell Reports Physical Science* **2022**, *3*, 101043.
(25) Dixit, M. B.; Zaman, W.; Hortance, N.; Vujic, S.; Harkey, B.; Shen, F.; Tsai, W.-Y.; De Andrade, V.; Chen, X. C.; Balke, N.; et al. Nanoscale mapping of extrinsic interfaces in hybrid solid electrolytes. *Joule* **2020**, *4*, 207−221.
(26) Eckhardt, J. K.; Fuchs, T.; Burkhardt, S.; Klar, P. J.; Janek, J.; Heiliger, C. Guidelines for Impedance Analysis of Parent Metal Anodes in Solid-State Batteries and the Role of Current Constriction at Interface Voids, Heterogeneities, and SEI. *Advanced Materials Interfaces* **2023**, *10*, No. 2202354.
(27) Fuchs, T.; Haslam, C. G.; Richter, F. H.; Sakamoto, J.; Janek, J. Evaluating the use of critical current density tests of symmetric lithium transference cells with solid electrolytes. *Adv. Energy Mater.* **2023**, *13*, No. 2302383.
(28) Eckhardt, J. K.; Klar, P. J.; Janek, J.; Heiliger, C. Interplay of dynamic constriction and interface morphology between reversible metal anode and solid electrolyte in solid state batteries. *ACS Appl. Mater. Interfaces* **2022**, *14*, 35545−35554.
(29) Vishnugopi, B. S.; Naik, K. G.; Kawakami, H.; Ikeda, N.; Mizuno, Y.; Iwamura, R.; Kotaka, T.; Aotani, K.; Tabuchi, Y.; Mukherjee, P. P. Asymmetric Contact Loss Dynamics during Plating and Stripping in Solid-State Batteries. *Adv. Energy Mater.* **2023**, *13*, No. 2203671.
(30) Kasemchainan, J.; Zekoll, S.; Spencer Jolly, D.; Ning, Z.; Hartley, G. O.; Marrow, J.; Bruce, P. G. Critical stripping current leads to dendrite formation on plating in lithium anode solid electrolyte cells. *Nature materials* **2019**, *18*, 1105−1111.
(31) Spencer Jolly, D.; Ning, Z.; Hartley, G. O.; Liu, B.; Melvin, D. L.; Adamson, P.; Marrow, J.; Bruce, P. G. Temperature dependence of lithium anode voiding in argyrodite solid-state batteries. *ACS Appl. Mater. Interfaces* **2021**, *13*, 22708−22716.
(32) Eckhardt, J. K.; Fuchs, T.; Burkhardt, S.; Klar, P. J.; Janek, J.; Heiliger, C. 3D impedance modeling of metal anodes in solid-state batteries−incompatibility of Pore Formation and constriction effect in physical-based 1D circuit models. *ACS Appl. Mater. Interfaces* **2022**, *14*, 42757−42769.
(33) Dixit, M. B.; Vishugopi, B. S.; Zaman, W.; Kenesei, P.; Park, J.-S.; Almer, J.; Mukherjee, P. P.; Hatzell, K. B. Polymorphism of garnet solid electrolytes and its implications for grain-level chemo-mechanics. *Nat. Mater.* **2022**, *21*, 1298−1305.

https://doi.org/10.1021/acsenergylett.4c00744
ACS Energy Lett. 2024, 9, 2387−2393